ACS APPLIED MATERIALS & INTERFACES

Research Article

www.acsami.org

Choline Derivate-Modified Doxorubicin Loaded Micelle for Glioma Therapy

Jianfeng Li,[†] Huiying Yang,[‡] Yujie Zhang,[†] Xutao Jiang,[†] Yubo Guo,[†] Sai An,[†] Haojun Ma,[†] Xi He,[†] and Chen Jiang*[,†,§]

[†]Key Laboratory of Smart Drug Delivery (Fudan University), Ministry of Education, Department of Pharmaceutics, School of Pharmacy, Fudan University 826 Zhangheng Road, Shanghai 201203, China

[‡]Department of Clinical Pharmacy and Pharmaceutical Management, School of Pharmacy, Fudan University 826 Zhangheng Road, Shanghai 201203, China

[§]State Key Laboratory of Medical Neurobiology, Fudan University, Shanghai 201203, China

Supporting Information

ABSTRACT: Ligand-mediated polymeric micelles have enormous potential for improving the efficacy of glioma therapy. Linear−dendritic drug−polymer conjugates composed of doxorubicin (DOX) and polyethylene glycol (PEG) were synthesized with or without modification of choline derivate (CD). The resulting MeO−PEG−DOX_8 and CD−PEG−DOX_8 could self-assemble into polymeric micelles with a nanosized diameter around 30 nm and a high drug loading content up to 40.6 and 32.3%, respectively. The optimized formulation 20% CD−PEG−DOX_8 micelles had superior cellular uptake and antitumor activity against MeO−PEG−DOX_8 micelles. The subcellular distribution using confocal study revealed that 20% CD−PEG−DOX_8 micelles preferentially accumulated in the mitochondria. Pharmacokinetic study showed area under the plasma concentration−time curve (AUC_{0-t}) and C_{max} for 20% CD−PEG−DOX_8 micelles and DOX solution were 1336.58 ± 179.43 mg/L·h, 96.35 ± 3.32 mg/L and 1.40 ± 0.19 mg/L·h, 1.15 ± 0.25 mg/L, respectively. Biodistribution study showed the DOX concentration of 20% CD−PEG−DOX_8 micelles treated group at 48 h was 2.37-fold higher than that of MeO−PEG−DOX_8 micelles treated group at 48 h and was 24 fold-higher than that of DOX solution treated group at 24 h. CD−PEG−DOX_8 micelles (20%) were well tolerated with reduced cardiotoxicity, as evaluated in the body weight change and HE staining studies, while they induced most significant antitumor activity with longest media survival time in an orthotopic mouse model of U87-luci glioblastoma model as displayed in the bioluminescence imaging and survival curve studies. Our findings consequently indicated that 20% CD−PEG−DOX_8 micelles are promising drug delivery system for glioma chemotherapy.

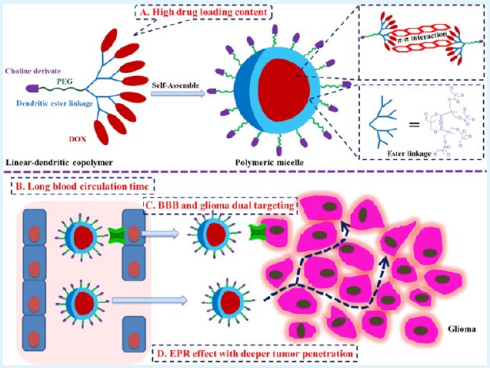

KEYWORDS: *choline derivate, linear−dendritic, drug−polymer conjugate, polymeric micelles, doxorubicin, glioma*

INTRODUCTION

With the rapid progress of nanotechnology, nanomedicines have sparked a rapidly growing interest as they have shown great promise to overcome intrinsic limitations associated with small molecule chemotherapeutic drugs, such as poor water solubility, undesired pharmacokinetics, and severe side effects.[1−3] Among them, drug−polymer conjugates and nanoparticles have been explored as drug carriers for delivery of chemotherapeutic drugs. Due to their tunable particle sizes and surface properties, these drug delivery systems are regarded as the hot area of anticancer research, especially in combination of advantages of both drug−polymer conjugates and nanoparticles.[4−7]

Some drug−polymer conjugates including antibody drug conjugates (ADC) with well-defined structures have reached the clinical trials.[8,9] The solubility of chemotherapeutic drugs could be increased by covalent linkage to water-soluble polymers like *N*-(2-hydroxypropyl) methacrylamide (HPMA) and poly(ethylene glycol) (PEG).[10,11] The tumor specificity could be improved by conjugation to tumor targeting antibodies. Well-defined structure, prolonged blood circulating time, and specific tumor targeting contributed to the superior antitumor effects. However, in order to avoid the fast renal clearance and maximize the tumor targeting, these polymers or antibodies are often designed to have molecular weights higher than 30−40 kDa, thus leading to relatively low drug loading content.[12,13] The exposure of payloads to the plasma may cause drug degradation. Besides, the large amount use of polymers or antibodies not only increases the cost, but also potentially

Received: August 1, 2015
Accepted: September 10, 2015
Published: September 10, 2015

DOI: 10.1021/acsami.5b07045
ACS Appl. Mater. Interfaces 2015, 7, 21589−21601

imposes safety issues.[14,15] Thus, these major problems remain to be solved for the optimum design of drug delivery systems.

Nanoparticles are also promising drug delivery systems that have been widely studied in both preclinical and clinical trials for systemic cancer treatment. Among them, polymeric micelles are of particular interest.[16−20] Polymeric copolymers with appropriate hydrophobic to hydrophilic ratios could self-assemble into core−shell micelles. The chemotherapeutic drugs can be encapsulated inside the hydrophobic core with high drug loading content and protected from degradation. The drug loaded micelles could accumulate preferentially in solid tumors through enhanced permeability and retention (EPR) effect. Besides, the sides effects could be avoid by the alerted biodistribution. However, the burst dilution, plasma protein adsorption, high blood flow shear stress, and uptake by kupffer cell or reticuloendothelial system could lead to instability of micelles.[21−27] Thus, the in vivo stability of micelles should be further improved.

The ideal drug delivery systems should integrate the advantages of drug−polymer conjugates and micelles including well-defined structure, long blood circulation time, specific tumor targeting and high drug loading content. Polymeric copolymers with various architectures, including linear and linear−dendritic copolymers, have been explored as drug carriers.[28−32] Compared with linear amphiphilic block copolymers, linear−dendritic copolymers are a unique class of polymers with good biocompatibility, well-defined structure and tunable aggregation properties. Due to more easily deform and reptate through the pores of the renal, the linear−dendritic architecture has superior in vivo stability against the linear one.[33,34] Given that linear−dendritic copolymers have tunable aggregation properties, the combination of linear hydrophilic and dendritic hydrophobic blocks or of linear hydrophobic and dendritic hydrophilic blocks has proven to be a promising approach to build amphiphilic copolymers that can self-assemble into micelles with high drug loading content.[35,36] The tumor-specific targeting could be achieved by introducing the targeting moiety to one end of polymer. Taking these together, we could integrate the advantages of linear−dendritic architecture and tunable aggregation property by using water-soluble polymers as hydrophilic segments and chemotherapeutic drugs as hydrophobic segments, which are covalently linked to water-soluble polymers. The water-soluble polymers could be further modified with targeting ligand. These amphiphilic drug−polymer conjugates could self-assemble into micelles as ideal drug delivery systems.

Glioma, the most common intracranial tumor, is considered as an incurable disease due to its high mortality and poor prognosis. Many classic and effective chemotherapeutics cannot reach the glioma due to the poor drug penetration caused by the vascular/tumor barrier such as blood−brain tumor barrier (BBTB) and blood−brain barrier (BBB). Some of the BBTB derived from normal brain microvessels retain some features of BBB and have smaller pores than other solid tumor.[37] As compared with other nanomedicines, micelles (in the sub-100 nm range) could penetrate and accumulate more effectively in solid tumors (such as pancreatic and glioma tumors) due to their small sizes.[38,39] The dual targeting to BBB and glioma could be achieved by targeting ligand. Thus, drug−polymer conjugates with BBB targeting moiety which could self-assemble into micelles could serve as ideal drug delivery systems for glioma therapy.

In this study, we proposed a novel polymeric micelle system for glioma therapy. Choline derivate (CD) with dual BBB and glioma transporter affinities was utilized as the targeting ligand.[40−42] PEG was chosen as the hydrophilic segment because it was the most widely used shell forming polymer that can prolong the blood circulation time of nanomedicines. Besides, it was one of the safe polymers approved by the Food and Drug Administration. Doxorubicin (DOX), an anthracycline antibiotic, was selected as the model drug and hydrophobic segment. It was among the most widely used anticancer agents that inhibited the growth of many cancerous cell lines, including glioblastoma.[43,44] Besides, the florescent nature ensured the precise tracking of the micelles. DOX was covalently linked to eight hydroxyl ends of PEG through carbonate bonds. Two drug-conjugating polymers, CD−PEG−DOX_8 and MeO−PEG−DOX_8, were synthesized and characterized. The micelles were prepared via a dialysis method. The particle size, in vitro release, cellular uptake, and intracellular distribution were investigated. The formulation was optimized in the pharmacokinetics study. The biodistribution, tumor accumulation, antitumor activity, and cytotoxicity were fully evaluated.

MATERIALS AND METHODS

MeO−PEG−OH (MW 5 kDa) was purchased from Yuanye Technology (Shanghai, China). Doxorubicin HCl was obtained from melonepharma (Dalian, China). CD was synthesized as published previously.[40] Other reagents, if not specified, were purchased from Sigma-Aldrich and used without purification.

Synthesis and Characterization of MeO−PEG−DOX_8 and CD−PEG−DOX_8. MeO−PEG−OH_8 was synthesized as previously described, comprising a 5 000 MW PEG segment and 8 hydroxyl groups.[45] Attachment of CD was performed as below.

MAL−PEG−OH with a molecular weight of 5 kDa (360 mg, 1 equ.) and CD (99 mg, 2 equiv) was dissolved in 3 mL of MeOH and the reaction mixture was stirred overnight at room temperature. The excess CD was purified by dialysis against H_2O using a Green bird membrane (MWCO = 3500), followed by distillation to afford 380 mg of CD−PEG−OH. The final product was characterized by ^{1}H NMR which was recorded on a Bruker AMX-600 NMR spectrometer, using tetramethylsilane (TMS) as an internal standard and $(CD_3)_2SO$ as solvent.

CD−PEG−OH (380 mg, 1 equiv) was dissolved in 4 mL of CH_2Cl_2. Benzylidene-2,2-bis(oxymethyl) propionic Anhydride (90 mg, 2 equiv) and DMAP (6 mg, 0.4 equiv) was added. Then, the reaction mixture was stirred for 6 h at room temperature. The excess anhydride was quenched by adding 1 mL of MeOH. After stirring for another 5 h, the mixture was precipitated into 250 mL of diethyl ether. The precipitate was filtered to afford the product as a white powder. The benzylidene protection was removed by acidic hydrolysis. The white powder was dissolved in 4 mL of 1 N HCl and reacted for 5 h at room temperature. The product was purified by dialysis against H_2O, followed by distillation to afford 300 mg of CD−PEG−OH_2.

CD−PEG−OH_2 (300 mg, 1 equiv) was dissolved in 4 mL of CH_2Cl_2. Benzylidene-2,2-bis(oxymethyl) propionic Anhydride (275 mg, 8 equiv) and DMAP (18 mg, 1.6 equiv) was added. Then the reaction mixture was stirred for 15 h at room temperature. The excess anhydride was quenched by adding 1 mL of MeOH. After stirring for another 7 h, the mixture was precipitated into 250 mL of diethyl ether. The precipitate was filtered to afford the product as a white powder. The benzylidene protection was removed by acidic hydrolysis. The white powder was dissolved in 4 mL of 1 N HCl and reacted for 15 h at room temperature. The product was purified by dialysis against H_2O, followed by distillation to afford 230 mg of CD−PEG−OH_4.

CD−PEG−OH_4 (230 mg, 1 equiv) was dissolved in 4 mL of CH_2Cl_2. Benzylidene-2,2-bis(oxymethyl) propionic Anhydride (326 mg, 20 equiv) and DMAP (19 mg, 4 equiv) was added. Then the

DOI: 10.1021/acsami.5b07045
ACS Appl. Mater. Interfaces 2015, 7, 21589−21601

reaction mixture was stirred for 15 h at room temperature. The excess anhydride was quenched by adding 1 mL of MeOH. After stirring for another 8 h, the mixture was precipitated into 250 mL of diethyl ether. The precipitate was filtered to afford the product as a white powder. The benzylidene protection was removed by acidic hydrolysis. The white powder was dissolved in 4 mL of 1 N HCl and reacted for 24 h at room temperature. The product was purified by dialysis against H_2O, followed by distillation to afford 130 mg of CD−PEG−OH_8. The final product was characterized by ^{1}H NMR as described above.

MeO−PEG−OH_8 (150 mg, 1 equiv) was dissolved in 8 mL of CH_2Cl_2, and pyridine (650 μL, 320 equiv) was added, followed by 4-nitrophenyl chloroformate (820 mg, 160 equiv). The reaction mixture was stirred at room temperature overnight, and then the white solid was filtered off and washed with CH_2Cl_2. Then, the product was precipitated into 200 mL of diethyl ether. The resulting white powder was filtered to afford the product as well as some excess 4-nitrophenyl chloroformate and pyridinium chloride. The resulting white solid (70 mg, 1 equiv) was dissolved in 2 mL of anhydrous *N*,*N*-dimethylformamide (DMF), and DOX HCl (119 mg, 20 equiv) was added, followed by triethylamine (54.8 μL, 40 equiv). The reaction mixture was then stirred in the dark for 24 h. The product was purified by preparative SEC (Sephadex LH20, GE Healthcare) in 99:1 methanol/acetic acid. The high-molecular-weight fractions were purified further by preparative SEC (Sephadex G25, GE Healthcare) in water. The high-molecular-weight fraction was lyophilized to provide MeO−PEG−DOX_8 as a red powder (78 mg). The final product was characterized by ^{1}H NMR. The amount of DOX conjugated to the copolymer was determined by measuring the absorbance at 488 nm of a solution of copolymer in water, using an extinction coefficient for DOX of 11 500 $L \cdot mol^{-1} \cdot cm^{-1}$.[13] The weight-average molecular weight (M_w) and polydispersity index were measured by gel permeation chromatography (GPC, Polymer Laboratories Inc.). The polymer was dissolved in tetrahydrofuran. Polystyrene standards were used to generate the calibration curve. These tests were conducted using tetrahydrofuran as a carrier solvent at 35 °C with a flow rate of 1 mL/min.

CD−PEG−OH_8 (130 mg, 1 equiv) was dissolved in 6 mL of CH_2Cl_2, and pyridine (435 μL, 320 equiv) was added, followed by 4-nitrophenyl chloroformate (548 mg, 160 equiv). The reaction mixture was stirred at room temperature overnight, and then the white solid was filtered off and washed with CH_2Cl_2. Then the product was precipitated into 200 mL of diethyl ether. The resulting yellow solid like product was filtered and dried on vacuum. The resulting product was dissolved in 2 mL of anhydrous DMF, and DOX HCl (128 mg, 20 equiv) was added, followed by triethylamine (59 μL 40 equiv). The reaction mixture was then stirred in the dark for 24 h. The product was purified as described above. The high-molecular-weight fraction was lyophilized to provide CD−PEG−DOX_8 as a red powder (65 mg). The final product was characterized by ^{1}H NMR and GPC as described above. The amount of DOX conjugated to the copolymer was also determined spectroscopically.

Preparation and Characterization of MeO−PEG−DOX_8 and CD−PEG−DOX_8 Micelles. The micelles were prepared via a dialysis method. Briefly, 5 mg of MeO−PEG−DOX_8 or CD−PEG−DOX_8 was dissolved in 1 mL of DMF and dialysis against H_2O for 24 h. The micellar solutions were then filtered through 0.22 μm filters and stored at 4 °C. For micelles with different CD−PEG−DOX_8 weight ratios (*n* % CD−PEG−DOX_8, *n* = 10, 20, 40), a mixture of 1−*n* % of MeO−PEG−DOX_8 and *n*% of CD−PEG−DOX_8 was dialysis against H_2O to obtain the designed micelles.

The morphologies of the micelles were observed by transmission electron microscopy (TEM; Tecnai G2 spirit Biotwin, FEI). A drop of MeO−PEG−DOX_8 or 20% CD−PEG−DOX_8 micellar solution was deposited on a carbon-coated copper grid and excess solutions were tapped with a filter paper. Then, the grid was dried at room temperature before visualization.

Cellular Uptake. U87-luci cells were obtained from American Type Culture Collection (ATCC, Rockville, MD, USA) and cultured at 37 °C in a humidified 5% CO_2 atmosphere. Growth medium was Dulbecco's modified Eagle's medium (DMEM) which supplemented with 10% fetal bovine serum (FBS), 100 U/mL penicillin, and 100 μg/mL streptomycin. U87-luci cells were seeded at a density of 5×10^4 cells/well in 6-well plates (Corning-Coaster, Tokyo, Japan). Cells were incubated for 24 h and checked under the microscope for confluency and morphology. Then, cells were incubated with DOX, MeO−PEG−DOX_8 or 20% CD−PEG−DOX_8 micelles with equal DOX concentration of 10 μg/mL for 4 h at 37 °C, respectively. Free excessive CD (1 mM) was also added to block the targeting effect. Then, cells were digested, centrifuged, and washed twice with PBS. The fluorescence intensity was analyzed using a flow cytometer (FACSCalibur, BD Biosciences, Bedford, MA) equipped with an argon ion laser (488 nm) as the excitation source. The cells without any treatment used as the control. For each flow cytometer analysis, 1×10^4 events were collected and data were analyzed using BD FACSDiva software (BD Biosciences).

Cytotoxicity Assay. The cytotoxicity of DOX, MeO−PEG−DOX_8 and 20% CD−PEG−DOX_8 micelles against U87-luci cells was evaluated by MTT assay. Cells were seeded at a density of 5×10^3 cells/well in a 96-well plate. After 24 h incubation, cells were then washed twice with Hank's solution and exposed to 160 μL of different concentrations of DOX, MeO−PEG−DOX_8 or 20% CD−PEG−DOX_8 micelles at 37 °C for 48 h. To assess cell viability, 40 μL of MTT (2.5 mg/mL) solution was added into each well and incubated at 37 °C for 2 h. The medium was removed and 100 μL of DMSO was added to each well to dissolve the formazan crystals formed by the living cells. Cells without treatment were served as control. Absorbance was read at 570 nm and corrected at 630 nm by dual wavelength detection using a Multiskan MK3 microplate reader (Thermo Scientific). Cell viability was calculated as the survival percentage of control.

Subcellular Distribution. U87-luci cells were seeded at a density of 5×10^4 cells/well in a 15 mm glass bottom cell culture dish (NEST, Wuxi, China). Cells were incubated for 24 h and checked under the microscope for confluency and morphology. Then cells were incubated with DOX or 20% CD−PEG−DOX_8 micelles with equal DOX concentration of 10 μg/mL for 2 or 24 h at 37 °C, respectively. Ten micorliters (10 μL) of of Hochest 33342 (1 μg/mL in Water) and 1 μL of Mito Tracer Red FM (0.5 μg/mL in DMSO) was added 10 min before imaging. Cells were examined using a confocal microscopy (Carl Zeiss LSM710, Germany).

Pharmacokinetics and Biodistribution Studies. The pharmacokinetics of different DOX formulations were detected in SD rats administered intraveinously (iv) via the tail vein at a dose of 5 mg DOX-equiv/kg (n = 6). The blood samples of each group were collected in heparinized tubes at different time point (0.083, 0.25, 0.5 1, 2, 4, 8, 12, 24, 48 h). The biodistribution study was performed in U87-luci-bearing nude mice. For xenograft model, nude mice were anaesthetized by intraperitoneal (ip) injection of 10% chloral hydrate. U87-Luci cells (1×10^5 in 5 μL PBS) were implanted into the right striatum (1.8 mm right lateral to the bregma and 3 mm of depth) of the mice by using a stereotactic fixation device with mouse adaptor. At the 28th day after implantation, model mice received DOX solution, MeO−PEG−DOX_8 and 20% CD−PEG−DOX_8 micelles at a dose of 5 mg DOX-equiv/kg (n = 4). Mice were sacrificed by cervical dislocation (2, 24, and 48 h after administration), and their main organs were excised, washed with cold saline, dried over filter paper, weighed, and frozen at −80 °C until analysis. All animal experiments were carried out in accordance with guidelines evaluated and approved by the ethics committee of Fudan University, Shanghai, China.

Determination of DOX was performed after acid hydrolysis to release doxorubicinone from polymer-bound DOX followed by HPLC.[46] Briefly, 50 μL of plasma sample or 10% (w/v) tissue homogenate was exposed to 50 μL of 4 M HCl at 60 °C for 0.5 h. Then, 200 μL of MeOH was added to precipitate the proteins. Following centrifugation twice (12 000 rpm, 5 min), 20 μL of each sample was injected into HPLC (Agilent, ODS C18 column (4.6 × 250 mm, 5 μm particle size), 0.01 M KH_2PO_4/acetonitrile/acetic acid = 65:35:0.3 (v/v/v), 1.0 mL/min, RT, Ex/Em = 480/560 nm) for doxorubicinone quantification.

DOI: 10.1021/acsami.5b07045
ACS Appl. Mater. Interfaces 2015, 7, 21589−21601

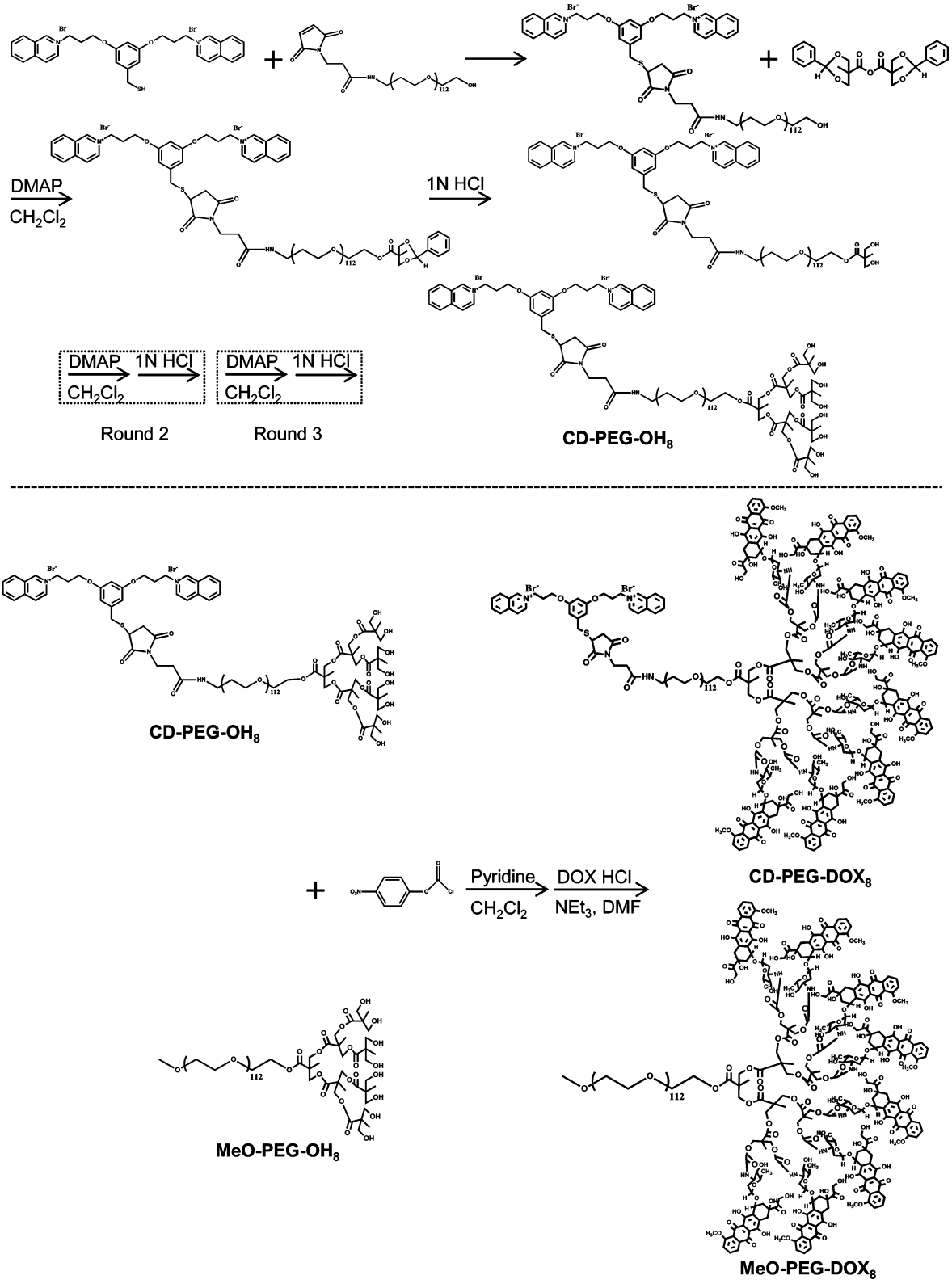

Figure 1. Synthetic route of MeO−PEG−DOX_8 and CD−PEG−DOX_8.

Tumor Distribution. At the 28th day after implantation, model mice received DOX solution, MeO−PEG−DOX_8 and 20% CD−PEG−DOX_8 micelles at a dose of 5 mg DOX-equiv/kg. Mice were sacrificed by cervical dislocation 48 h after administration, and the excised brain tumors were fixed in 4% paraformaldehyde for 48 h, placed in 15% sucrose PBS solution for 24 h until subsidence, then in 30% sucrose for 48 h until subsidence. Afterward, brain tumors were frozen in OCT embedding medium (Sakura, Torrance, CA) at −80 °C. Frozen sections of 20 μm thickness were prepared with a cryotome Cryostat (Leica, CM 1900, Wetzlar, Germany) and stained with 300 nM DAPI for 10 min at room temperature. The slides were mounted with coverslips and visualized with a confocal microscopy.

Antitumor Efficacy. U87-Luci-bearing mice received three injections of DOX solution, MeO−PEG−DOX_8 and 20% CD−

DOI: 10.1021/acsami.5b07045
ACS Appl. Mater. Interfaces 2015, 7, 21589−21601

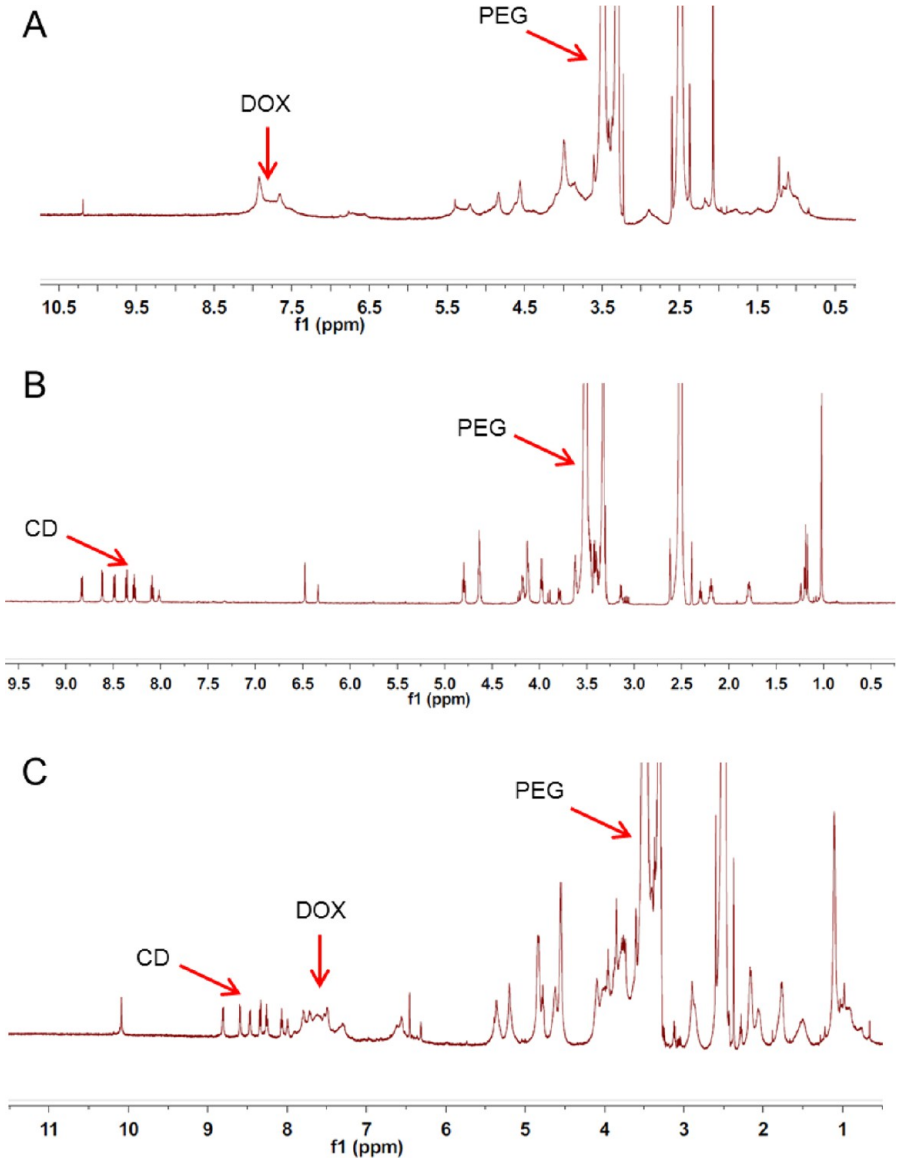

Figure 2. ^{1}H NMR spectrum of (A) MeO−PEG−DOX$_8$, (B) CD−PEG−OH$_8$, and (C) CD−PEG−DOX$_8$. The red arrows indicate the specific peak of each segment.

PEG−DOX$_8$ micelles at a dose of 5 mg DOX-equiv/kg on days 14, 21, and 28. Control groups received PBS only. Mice were imaged noninvasively for luciferase expression 2 days after each injection (days 16, 23, and 30). Briefly, 150 mg/kg D-luciferin was administered via intraperitoneal injection, and mice were anesthetized with 1% isoflurane/oxygen mixture. Then, bioluminescence imaging was obtained at 15 min post luciferin injection using IVIS Spectrum with Living Image software 4.2 (Caliper Life Science). The quantitative total bioluminescence was measured by drawing regions of interest (ROIs) around tumor areas enclosing emitted signals. Background was subtracted by measuring same sized ROIs in areas without light emission (n = 3). For survival study, all groups were inspected twice daily. Survival time of the animals and body weights were also recorded (n = 12).

Toxicity Evaluation. U87-Luci-bearing mice received three injections of DOX solution, MeO−PEG−DOX$_8$ and 20% CD−PEG−DOX$_8$ micelles at a dose of 5 mg DOX-equiv/kg on days 14, 21, and 28. One day after the treatment, mice were sacrificed, and sections of the main organs were stained with hematoxylin and eosin.

RESULTS AND DISSCUSION

Design, Synthesis, and Characterization of MeO−PEG−DOX$_8$ and CD−PEG−DOX$_8$. In a general perspective, hydrophobic chemotherapeutics can be loaded into micelle delivery systems in a covalent or noncovalent manner.[47] Regardless of release profile, covalently loaded drugs have long blood circulation times, which could maximize the EPR effect.[38] Besides, it was possible to maintain the drug concentration inside the therapeutic window for longer time in the tumor tissue as compared to free drug. In our previous work, we synthesized an amphiphilic copolymer, MeO−PEG−RA$_8$ for the successful delivery of paclitaxel to breast cancer.[45] In this study, we designed a linear−dendritic copolymer composed of polyethylene glycol (PEG) and doxorubicin (DOX). This copolymer was further attached with targeting ligand CD and spontaneously assembled into micelle.

The overall synthetic route is shown in Figure 1. First, the targeting ligand CD was attached to MAL−PEG−OH via Michael addition. The amplification of hydroxyl ends achieved

DOI: 10.1021/acsami.5b07045
ACS Appl. Mater. Interfaces 2015, 7, 21589−21601

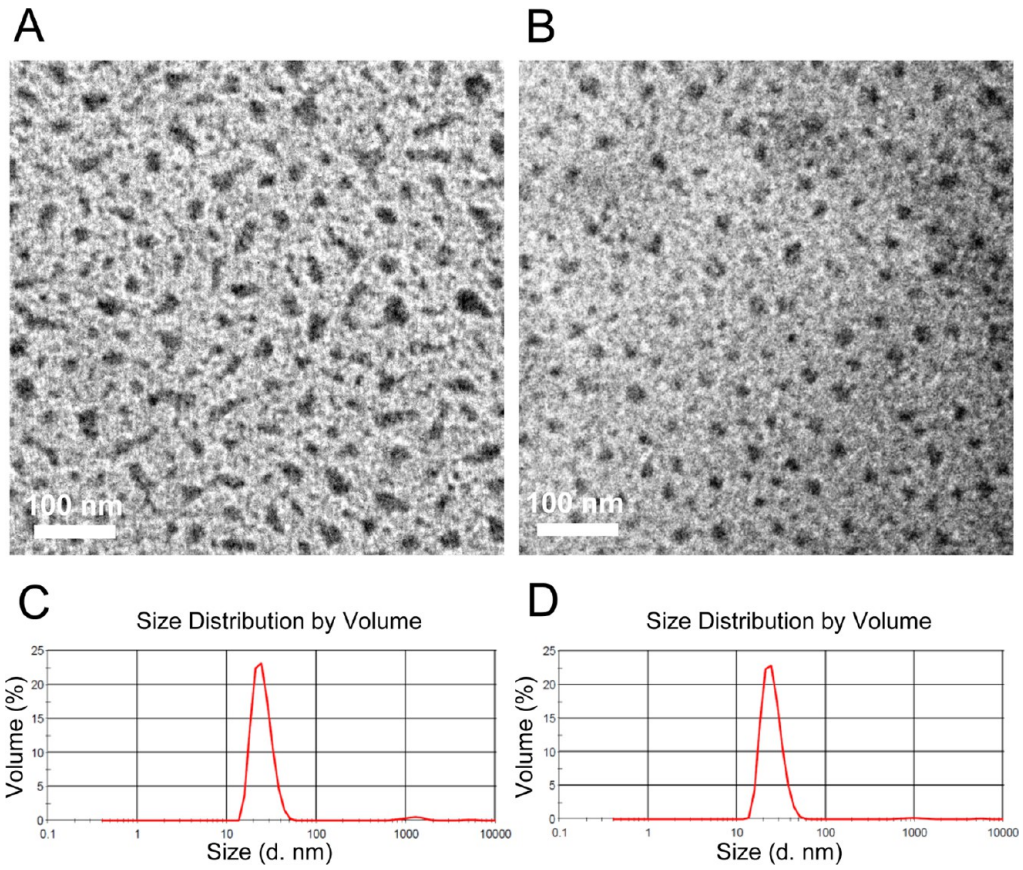

Figure 3. Characterization of micelles. Transmission electron microscopy (TEM) micrographs of (A) MeO−PEG−DOX_8 and (B) 20% CD−PEG−DOX_8 micelles. Particle size distribution of (C) MeO−PEG−DOX_8 and (D) 20% CD−PEG−DOX_8 micelles.

through three rounds of anhydride acylation and acetal hydrolysis, resulting CD−PEG−OH_8. Analysis of ^{1}H NMR spectrum showed the successful CD conjugation, with the appearance of CD isoquinoline protons observed (Figure 2B). Further analysis of the integration values indicated that CD−PEG−OH_8 contained 1.06 CD. DOX was conjugated to CD−PEG−OH_8 and MeO−PEG−OH_8 using 4-nitrophenyl chloroformate as a linker. And the resulting CD−PEG−DOX_8 and MeO−PEG−DOX_8 was characterized by ^{1}H NMR and GPC (Figure 2, Supporting Information Figure S1). Peaks between 7 and 8 ppm represented the protons of anthracene ring in DOX. Because of the overlapped integration, it was difficult to calculate the numbers of DOX conjugated to the copolymer. We utilized GPC and UV absorption at 488 nm to evaluate the conjugation efficiency. The DOX conjugation degree calculated from GPC results was 7.85 for MeO−PEG−DOX_8 and 6.05 for CD−PEG−DOX_8. The amount of DOX conjugated to copolymer was 40.6 and 32.3%. These results indicated the successful synthesis of liner-dendritic copolymers.

Preparation and Characterization of Micelles. Micelle structures formed spontaneously upon dialysis against ddH_2O. The TEM images showed both homogeneous sizes of MeO−PEG−DOX_8 and 20% CD−PEG−DOX_8 micelles (Figure 3A,B). The optimization of CD conjugation was discussed in the pharmacokinetic studies. Both micelle formulations were around 30 nm, as determined by DLS (Figure 3C,D). Using a dialysis method, DOX solution showed a rapid release of 40% of the drug in the first hour, and the total release was almost 90% by 24 h. However, MeO−PEG−DOX_8 or 20% CD−PEG−DOX_8 micelles either exhibited slow drug release, with cumulative release less than 10% of the drug by 24 h in PBS solutions (Supporting Information Figure S2).

Cellular Uptake. The cellular uptake of DOX solution, MeO−PEG−DOX, and 20% CD−PEG−DOX_8 micelles into U87-luci cells was analyzed by flow cytometry. CD−PEG−DOX_8 micelle showed higher fluorescent intensity than MeO−PEG−DOX_8 micelle which can be decreased by excessive CD. However, the fluorescent intensity of both micelles treated groups were much less than that of DOX solution treated group (Figure 4). Although DOX hydrochloride has high solubility in the aqueous solution (>10 mg/mL), the anthracene ring in the molecular structure endows its hydrophobic nature. It can diffuse through the cell membranes easily via a passive manner. Thus, the DOX solution had higher cellular accumulation than micelles treated groups.

Cytotoxicity Assay. The in vitro antitumor activity was determined by MTT assay as shown in Figure 5. The IC_{50} of each group was 14.62, 6.04, and 0.81 μg/mL for MeO−PEG−DOX_8, 20% CD−PEG−DOX_8 micelles, and DOX solution. This was consistent with cellular uptake results. The DOX solution treated group with highest cellular accumulation had the lowest IC_{50} value, and 20% CD−PEG−DOX_8 had higher antitumor activity than that of MeO−PEG−DOX_8.

Subcellular Distribution. Although micelle groups had lower cellular uptake and slow DOX release rate, they both exhibited moderate antitumor activity as compared with DOX solution. Herein, subcellular distribution was carried out to investigate the cytotoxicity mechanism of micelles. As shown in Figure 6, DOX distributed in both cytoplasm and nucleus regions after 2 h of incubation. DOX in the cytoplasm was

DOI: 10.1021/acsami.5b07045
ACS Appl. Mater. Interfaces 2015, 7, 21589−21601

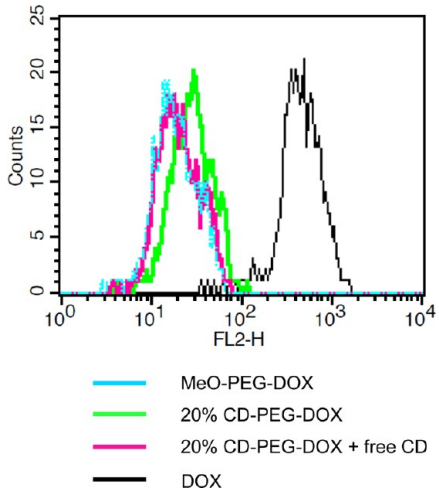

Figure 4. Flow cytometry profiles of cellular uptake in U87-luci cells treated by DOX solution, MeO−PEG−DOX_8, and 20% CD−PEG−DOX_8 micelles with equal DOX concentration of 10 mg/mL after 4 h of incubation. Cells without any treatment used as the control. Cells together with 20% CD−PEG−DOX_8 micelles and excessive CD treatment served as blocking group.

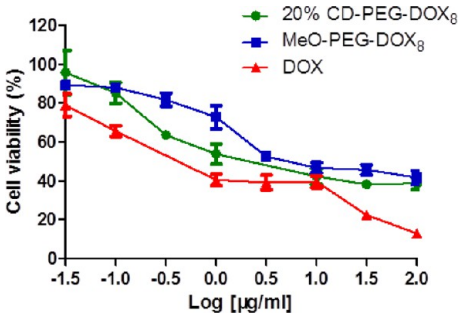

Figure 5. Cytotoxicity of DOX solution, MeO−PEG−DOX_8, and 20% CD−PEG−DOX_8 micelles against U87-luci cells. Data are represented as means ± SD (n = 4).

partially colocalized with the mitochondria which was stained by Mito Tracer Red. DOX in the nucleus was totally colocalized with Hoechst stained DNA. After 24 h incubation, the nuclear membranes became permeable. DOX and Mito Tracer Red were spread out in the whole cell. DOX itself could preferentially accumulate in the nuclear and insert into DNA to induce apoptosis. While 20% CD−PEG−DOX_8 appeared only in the cytoplasm in the first 2 h. It displayed total colocalization with the mitochondria, after 24 h of incubation, 20% CD−PEG−DOX_8 also appeared in the nucleus. Meanwhile, penetration of Mito Tracer Red into the nucleus indicated the leakage of the nuclear membranes. The common pathway of cellular internalization for micelles was endocytosis. However, 20% CD−PEG−DOX_8 showed obvious accumulation in mitochondria other than in lysosome. In the DNA mobility retardation study, CD−PEG−DOX_8 was proved to intercalate into plasmid DNA at different weight ratios (Supporting Information Figure S3). The mitochondrial DNA may also be affected by CD−PEG−DOX_8. When the nuclear membrane became permeable, it could further accumulate into the chromosomal DNA and induce the tumor apoptosis together with released DOX. This could be the explanation for its cytotoxicity.

Pharmacokinetics Study. The long plasma half-lives of micelles could ensure the maximum beneficial of EPR effect and specific targeting for tumor accumulation. Micelles with different CD conjugation ratios may have different blood retention time. Thus, micelles with different CD−PEG−DOX_8 weight ratios (n% CD−PEG−DOX_8, n = 0, 10, 20, 40, 100) were iv injected into SD rats. The concentration of DOX in the plasma was measured at various time points (Figure 7) and the pharmacokinetic parameters were calculated using noncompartmental analysis (Table 1). Compared with DOX solution, all micelles retained in the blood circulation for long time except for 100% CD−PEG−DOX_8. The linear−dendritic structure, ester linkage, and the possible $\pi-\pi$ interaction between anthracene rings of DOX contributed to the high in vivo stability of micelles. The area under the plasma concentration−time curve (AUC(0−t)) and mean residence time (MRT(0−t)) decreased dramatically when the weight ratio of CD−PEG−DOX_8 reached 100%. While, there was no difference in the initial blood concentration and C_{max} of all micelle groups which were 100 times higher than those of the DOX solution group, respectively. The concentration of DOX in 100% CD−PEG−DOX_8 dropped to the same level of that in DOX solution group 2 h after injection. Make a balance between targeting and blood circulating time, 20% CD−PEG−DOX_8 with high AUC(0−t) and long MRT(0−t) was selected as the optimal micelle formulation.

Biodistribution Study. U87-Luci-bearing nude mice were administrated with DOX solution, MeO−PEG−DOX_8 and 20% CD−PEG−DOX_8 micelles. Then, DOX concentrations in main organs and tumors were measured at 2, 24, and 48 h after administration (Figure 8). For DOX solution treated group, DOX concentration in all organs decreased along with time. Because of the long circulating time, DOX concentration in micelles treated groups increased from 2 to 48 h. The drug accumulation was significantly greater at 48 h than that at 2 h, especially in tumors. The DOX concentration of 20% CD−PEG−DOX_8 micelle treated group at 48 h was 2.37-fold higher than that of MeO−PEG−DOX_8 micelle treated group at 48 h and was 24 fold-higher than that of DOX solution treated group at 24 h. This indicated the superiority of micellar formulation and targeting ligand. Another important phenomenon observed was the higher liver uptake of 20% CD−PEG−DOX_8 micelle than MeO−PEG−DOX_8 micelle at each point. This might be the explanation for dramatic blood concentration decrease of 100% CD−PEG−DOX_8 micelle treated group. The liver uptake could lead to fast clearance of 100% CD−PEG−DOX_8 micelle from the blood circulation. This was consistent with results of positron emission computed tomography (PET) imaging using FCH, which showed a high background signal in the liver.[48,49]

Tumor Distribution. To investigate the tumor penetration in the tumor and nearby heathy brain tissue, we examined tumor sections of DOX solution, MeO−PEG−DOX_8 and 20% CD−PEG−DOX_8 micelles treated groups under fluorescent microscope (Figure 9). In the perspective of fluorescent intensity, DOX was almost undetectable due to the rapid clearance from the blood circulation 48 h after administration. Both micelles showed obvious accumulation due to the EPR effect. 20% CD−PEG−DOX_8 micelle exhibited more tumor accumulation than MeO−PEG−DOX_8 micelle due to the targeting effect of CD ligand. In the perspective of fluorescent distribution, both micelles accumulated near the tumor edge. A similar tumor distribution was found using a CD modified

DOI: 10.1021/acsami.5b07045
ACS Appl. Mater. Interfaces 2015, 7, 21589−21601

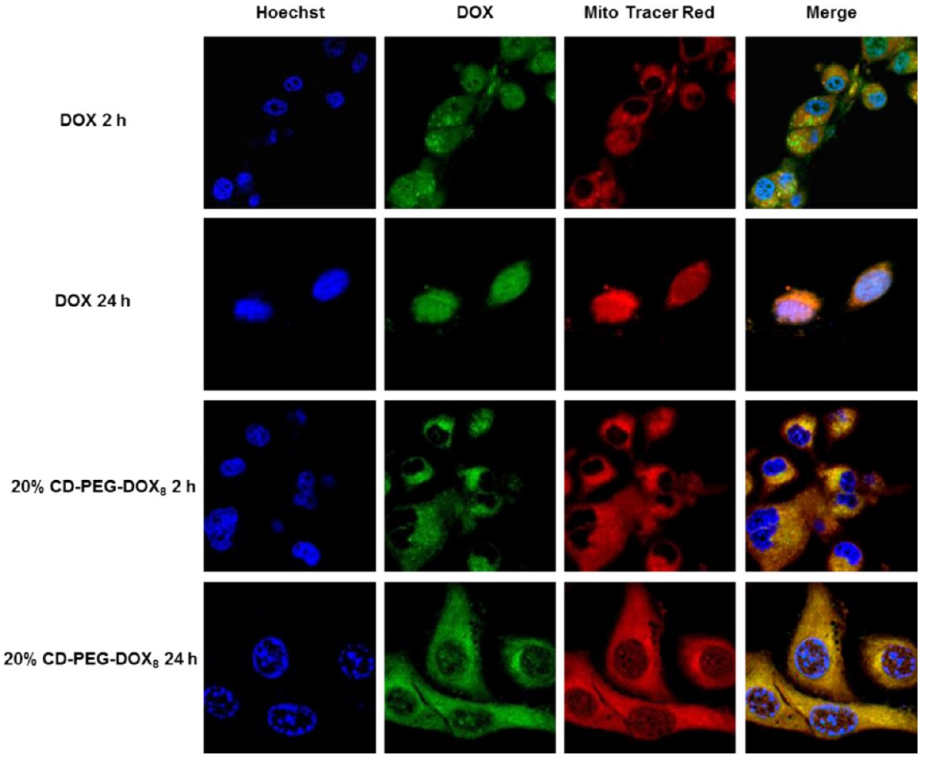

Figure 6. Subcellular distribution of DOX solution and 20% CD−PEG−DOX_8 micelle following incubation in U87-luci cells for 2 and 24 h. The cell nucleus was stained with Hoechst (blue) and the mitochondria was stained with Mito Tracer Red, respectively. The florescence of DOX was set as green color.

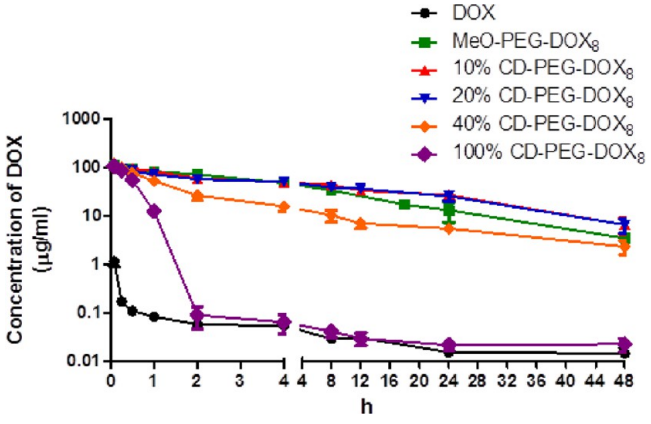

Figure 7. Pharmacokinetic profiles in SD rats after iv administration of DOX solution, MeO−PEG−DOX_8 and CD−PEG−DOX_8 with different CD ratios at a dose of 5 mg DOX-equiv/kg. Data are represented as means ± SD (n = 6).

nanoprobe which induced a ring-enhancing lesion. The hyperosmosis prevented the micelles from penetrating into deeper tumor regions.[42] This observation indicated that the treatment should be started at an earlier stage. Another concern should be the nonspecific accumulation of 20% CD−PEG−DOX_8 micelle in normal brain tissue because the choline transporter was also expressed in this region. Here, the fluorescent imaging showed little accumulation of 20% CD−PEG−DOX_8 micelle in brain tissue. One explanation was that both the expression and Vmax of choline transporters in tumors was higher than those in normal brain tissue.[50,51]

Antitumor Efficacy. U87-Luci-bearing glioma model had stable luciferase expression. When ip administrated with D-fluorescein sodium, the glioma region could release photons for bioluminescence imaging. This modality could offer a non-invasive and real-time way to monitor the tumor growth.[52] Nude mice bearing U87-luci glioma xenograft were received three iv injections of DOX solution, MeO−PEG−DOX_8 and 20% CD−PEG−DOX_8 micelles at a dose of 5 mg DOX-equiv/kg on days 14, 21, and 28. Bioluminescence imaging was performed on days 16, 23, and 30 and tumor bioluminescence was quantified by measuring pseudocolor intensity. The body weight change and median survival time were also monitored (Figure 10). Compared with the control group, mice in all treatment groups displayed significantly slower increase rates of

Table 1. Noncompartmental Analysis of Pharmacokinetic Parameters

parameter	DOX	MeO−PEG−DOX_8	10% CD−PEG−DOX_8	20% CD−PEG−DOX_8	40% CD−PEG−DOX_8	100% CD−PEG−DOX_8
AUC(0−t) (mg/L·h)	1.40 ± 0.19	966.58 ± 165.85[a]	1372.21 ± 202.68[a]	1336.58 ± 179.43[a]	417.05 ± 68.85[a]	67.05 ± 2.28[b]
MRT(0−t) (h)	14.11 ± 1.60	11.18 ± 2.21	15.01 ± 1.11	15.21 ± 0.40	12.00 ± 0.78	0.79 ± 0.07[b]
C_{max} (mg/L)	1.15 ± 0.25	106.90 ± 6.14[a]	111.49 ± 3.99[a]	96.35 ± 3.32[a]	116.68 ± 7.12[a]	105.49 ± 5.62[a]

[a] $P < 0.001$ compared with DOX solution. [b] $P < 0.001$ compared with other micelle groups. Data were statistically analyzed by one-way ANOVA with Bonferroni post-test.

DOI: 10.1021/acsami.5b07045
ACS Appl. Mater. Interfaces 2015, 7, 21589−21601

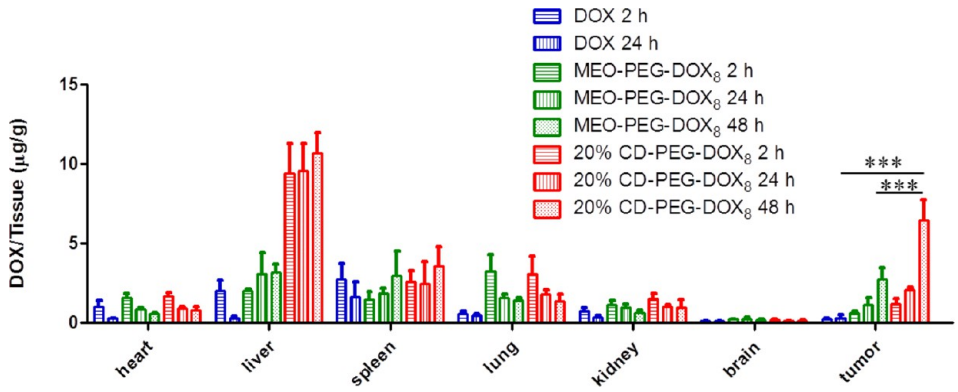

Figure 8. Distribution profiles of DOX in tissues of U87-luci-bearing mice after iv administration of DOX solution, MeO−PEG−DOX_8 and 20% CD−PEG−DOX_8 micelles at a dose of 5 mg DOX-equiv/kg. Data are represented as means ± SD (n = 4). Data were statistically analyzed by one-way ANOVA with Bonferroni post-test. ***P < 0.001 20% CD−PEG−DOX_8 micelle versus DOX solution or MeO−PEG−DOX_8 micelle.

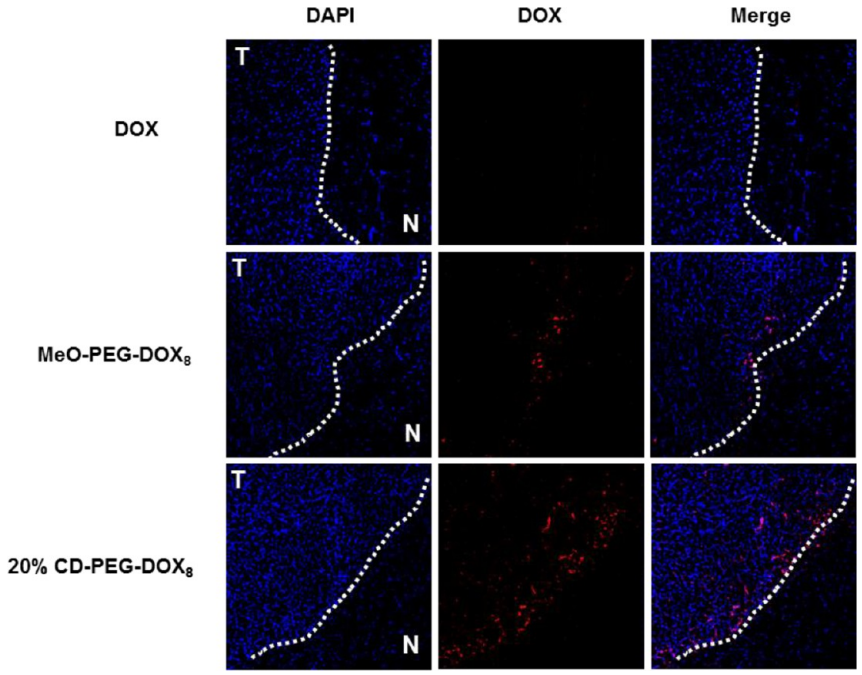

Figure 9. Tumor distribution of DOX solution, MeO−PEG−DOX_8 and 20% CD−PEG−DOX_8 micelles 48 h after iv administration. Brain tumor sections were imaged under confocal microscope. N, normal brain; T, glioma; dashed line, boundary of the glioma. The nucleus was stained by DAPI (blue), and red is the signal of DOX.

light intensity. Among these groups, light intensities in MeO−PEG−DOX_8 micelle treated groups were higher than those of DOX solution and 20% CD−PEG−DOX_8 micelle treated groups. While, DOX exhibited comparable tumor inhibition with 20% CD−PEG−DOX_8 micelle (Figure 10A and B). As estimated from pharmacokinetics and tissue distribution studies, DOX distributed into the whole body quickly and nonspecifically. The tumor accumulation was much lower than micelles. However, DOX itself could be efficiently concentrated into the nuclear to induce the cell apoptosis. Its therapeutic effect was confirmed by in vivo apoptosis detection using TUNEL assay (Supporting Information Figure S4). Compared with DOX group, the high AUC(0−t) and targeting efficacy contributed to the tumor accumulation of 20% CD−PEG−DOX_8 micelle, which remedied the relatively low in vitro cytotoxicity. Thus, 20% CD−PEG−DOX_8 micelle showed most significant antitumor activity. The median survival time was 47 days for 20% CD−PEG−DOX_8 micelle treated group, 41.5 days for MeO−PEG−DOX_8 micelle treated groups, 34.5 days for DOX solution treated group, and 33.5 days for saline treated group (Figure 10D). Although remarkable tumor inhibition and apoptosis were observed in DOX treated group, no benefit of median survival time emerged. Three doses of DOX solution caused 2 g of body weight loss on average. No obvious change was found in other groups (Figure 10C).

Toxicity Evaluation. A major bottleneck of using chemotherapy in clinical is its side effects. And sometimes these side effects are lethal for patients including the cardiotoxicity of DOX.[53] Most studies suggested that DOX can be catalyzed into semiquinone metabolites which can directly kill the cells. At the same time, large amounts of free radicals in the metabolic process binding to proteins, nucleic acids, and macromolecules could further cause cell damage. Besides, DOX had high binding affinity to the myocardial cardiolipin. This could lead to sustained damage to cardiac cells. To further evaluate the

DOI: 10.1021/acsami.5b07045
ACS Appl. Mater. Interfaces 2015, 7, 21589−21601

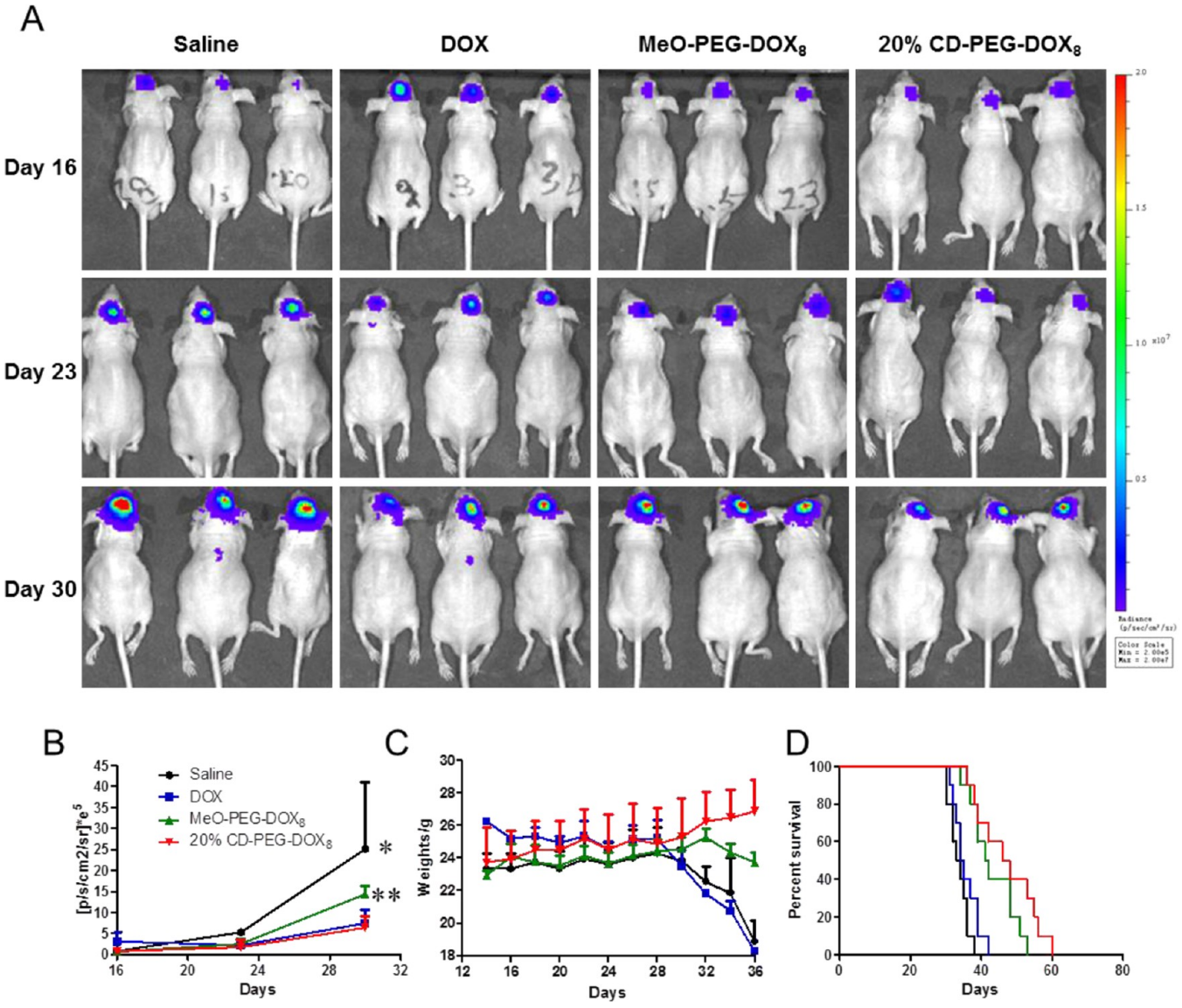

Figure 10. Antitumor efficacy after iv administration of different DOX formulations. U87-Luci-bearing mice received three injection of DOX solution, MeO−PEG−DOX_8, and 20% CD−PEG−DOX_8 micelles at a dose of 5 mg DOX-equiv/kg on days 14, 21, and 28. Control groups received PBS only. (A) Noninvasive bioluminescence imaging of U87-luci-bearing mice at different time points after treatment (day 16, 23, 30). (B) Quantification of signals from the entire abdominal region of each mouse (n = 3) Data were statistically analyzed by unpaired t test. *P < 0.05 and **P < 0.01 were considered significant. (C) Body weight change and (D) Kaplan−Meier survival curves of model mice (n = 12). Data are represented as means ± SD.

toxicities of different formulations, sections of main organs, including heart, liver, spleen, lung, and kidney, were stained with hematoxylin and eosin. As shown in Figure 11, green arrows in the heart section of DOX solution treated group indicated myocardial hypertrophy caused by DOX. An unexpected finding was the pneumonemia in the lung section of DOX solution treated group as reveled by black arrows. While having effective antitumor effect, DOX solution treatment did not improved the median survival time due to the above-mentioned toxicities. Another side effect may rise from the fast clearance of DOX from blood circulation. DOX could permeate out of the blood vessel wall resulting ulcer and necrosis of tissues.[54] For micelle treated groups, no obvious toxicities were found in liver even though micelle formulations had high liver accumulations. As the main metabolic organ, the liver can dispose a greater dose of DOX without affecting its normal function. Another inspiring result was that micelles also induced no obvious cardiotoxicity, regardless of comparable heart accumulation to DOX solution. The different intracellular fate may reduce the cardiotoxicity (Figure 6). Micelles also had no cytotoxicity in other organs. Together with improved tumor accumulation, reduced side effects maximized the therapeutic effect of 20% CD−PEG−DOX_8 micelle.

CONCLUSION

In this study, MeO−PEG−DOX_8 and 20% CD−PEG−DOX_8 micelles with high drug loading content were synthesized successfully. Micelles showed both high in vitro and in vivo stability due to the linear−dendritic architecture. Meanwhile, 20% CD−PEG−DOX_8 exhibited higher cellular uptake and glioma accumulation than MeO−PEG−DOX_8. Moreover, the altered intracellular distribution and improved biodistribution reduced the cytotoxicity of micelles. Taking those together,

DOI: 10.1021/acsami.5b07045
ACS Appl. Mater. Interfaces 2015, 7, 21589−21601

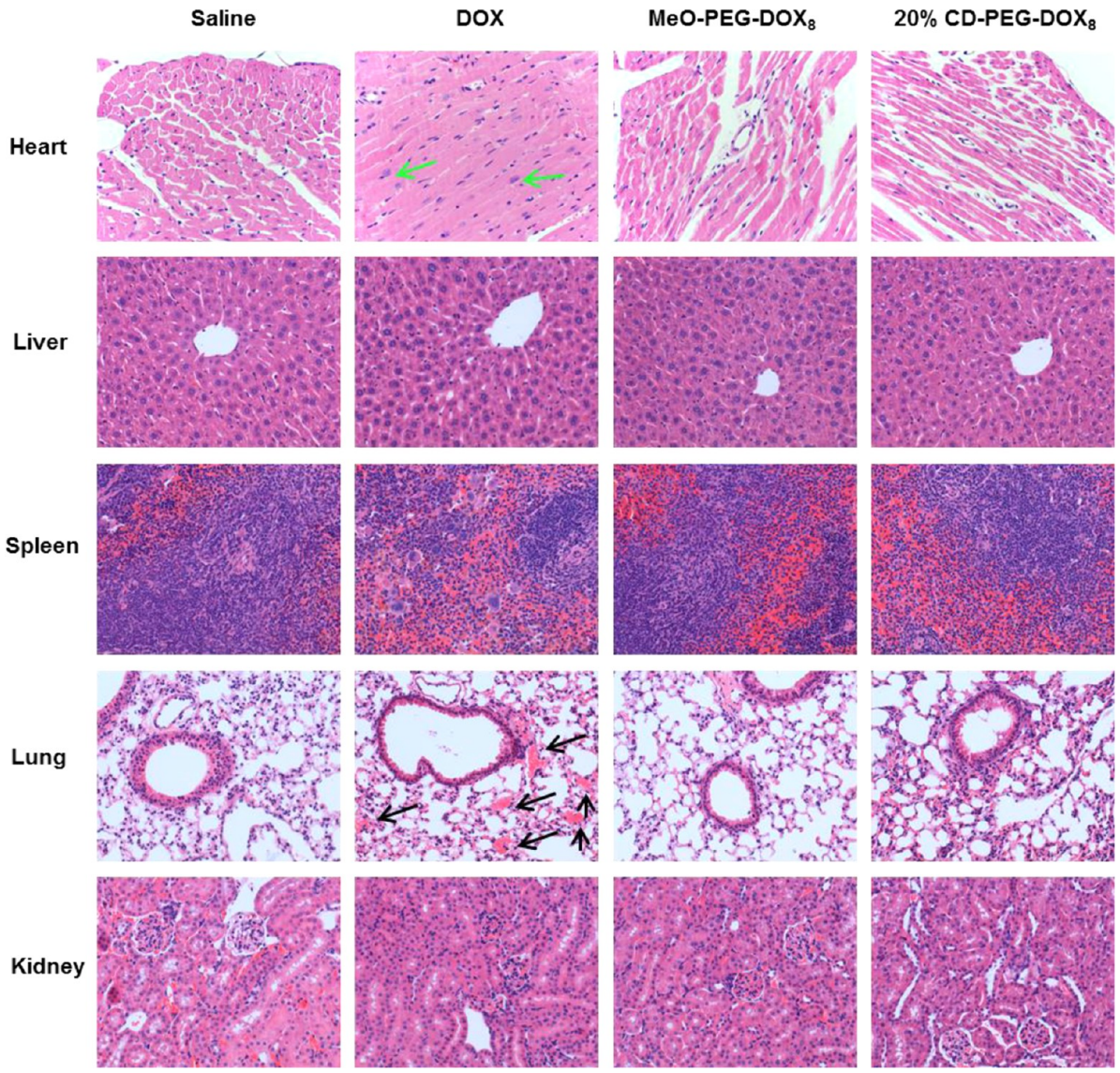

Figure 11. Toxicity evaluation after iv administration of different DOX formulations. Histochemistry analysis of heart, liver, spleen, lung, and kidney sections stained with hematoxylin and eosin. Green arrows indicate the myocardial hypertrophy, and black arrows indicate pneumonemia. Original magnification: 400×.

20% CD−PEG−DOX_8 maximized the therapeutic effects and minimized the side effects of DOX. This linear−dendritic polymer−drug conjugation with CD modification could be a promising platform for glioma chemotherapy.

■ ASSOCIATED CONTENT

Supporting Information

The Supporting Information is available free of charge on the ACS Publications website at DOI: 10.1021/acsami.5b07045.

GPC chromatograms of MeO−PEG−DOX_8 and 20% CD−PEG−DOX_8, in vitro release profiles, DNA mobility retardation assay, and apoptosis detection of tumor sections.(PDF)

■ AUTHOR INFORMATION

Corresponding Author

* Tel: +86 21 51980079. Fax: +86 21 51980079. E-mail: jiangchen@shmu.edu.cn.

Notes

The authors declare no competing financial interest.

■ ACKNOWLEDGMENTS

This work was supported by grants from the National Basic Research Program of China (973 Program, 2013CB932500), the National Natural Science Foundation of China (81172993), and the National Science Fund for Distinguished Young Scholars (81425023).

■ REFERENCES

(1) Torchilin, V. P. Multifunctional, Stimuli-Sensitive Nanoparticulate Systems for Drug Delivery. *Nat. Rev. Drug Discovery* **2014**, *13*, 813−827.

(2) Dawidczyk, C. M.; Kim, C.; Park, J. H.; Russell, L. M.; Lee, K. H.; Pomper, M. G.; Searson, P. C. State-of-the-Art in Design Rules for Drug Delivery Platforms: Lessons Learned from FDA-Approved Nanomedicines. *J. Controlled Release* **2014**, *187*, 133−144.

DOI: 10.1021/acsami.5b07045
ACS Appl. Mater. Interfaces 2015, 7, 21589−21601

(3) Xu, X.; Ho, W.; Zhang, X.; Bertrand, N.; Farokhzad, O. Cancer Nanomedicine: from Targeted Delivery to Combination Therapy. *Trends Mol. Med.* **2015**, *21*, 223−232.
(4) Haag, R.; Kratz, F. Polymer Therapeutics: Concepts and Applications. *Angew. Chem., Int. Ed.* **2006**, *45*, 1198−1215.
(5) Duncan, R. Drug-Polymer Conjugates: Potential for Improved Chemotherapy. *Anti-Cancer Drugs* **1992**, *3*, 175−210.
(6) Estanqueiro, M.; Amaral, M. H.; Conceicao, J.; Sousa Lobo, J. M. Nanotechnological Carriers for Cancer Chemotherapy: the State of the Art. *Colloids Surf., B* **2015**, *126*, 631−648.
(7) Poon, W.; Zhang, X.; Nadeau, J. Nanoparticle Drug Formulations for Cancer Diagnosis and Treatment. *Crit. Rev. Oncog.* **2014**, *19*, 223−245.
(8) Mack, F.; Ritchie, M.; Sapra, P. The Next Generation of Antibody Drug Conjugates. *Semin. Oncol.* **2014**, *41*, 637−652.
(9) Goncalves, A.; Tredan, O.; Villanueva, C.; Dumontet, C. Antibody-Drug Conjugates in Oncology: from the Concept to Trastuzumab Emtansine (T-DM1). *Bull. Cancer* **2012**, *99*, 1183−1191.
(10) Etrych, T.; Sirova, M.; Starovoytova, L.; Rihova, B.; Ulbrich, K. HPMA Copolymer Conjugates of Paclitaxel and Docetaxel with pH-Controlled Drug Release. *Mol. Pharmaceutics* **2010**, *7*, 1015−1026.
(11) Pasut, G.; Veronese, F. M. PEG Conjugates in Clinical Development or Use as Anticancer Agents: an Overview. *Adv. Drug Delivery Rev.* **2009**, *61*, 1177−1188.
(12) Schluep, T.; Hwang, J.; Cheng, J.; Heidel, J. D.; Bartlett, D. W.; Hollister, B.; Davis, M. E. Preclinical Efficacy of the Camptothecin-Polymer Conjugate IT-101 in Multiple Cancer Models. *Clin. Cancer Res.* **2006**, *12*, 1606−1614.
(13) Lee, C. C.; Gillies, E. R.; Fox, M. E.; Guillaudeu, S. J.; Frechet, J. M.; Dy, E. E.; Szoka, F. C. A Single Dose of Doxorubicin-Functionalized Bow-Tie Dendrimer Cures Mice Bearing C-26 Colon Carcinomas. *Proc. Natl. Acad. Sci. U. S. A.* **2006**, *103*, 16649−16654.
(14) Carter, P. J.; Senter, P. D. Antibody-Drug Conjugates for Cancer Therapy. *Cancer J. (Philadelphia, PA, U. S.)* **2008**, *14*, 154−169.
(15) Sassoon, I.; Blanc, V. Antibody-Drug Conjugate (ADC) Clinical Pipeline: a Review. *Methods Mol. Biol. (N. Y., NY, U. S.)* **2013**, *1045*, 1−27.
(16) Mohamed, S.; Parayath, N. N.; Taurin, S.; Greish, K. Polymeric Nano-Micelles: Versatile Platform for Targeted Delivery in Cancer. *Ther. Delivery* **2014**, *5*, 1101−1121.
(17) Nakayama, M.; Akimoto, J.; Okano, T. Polymeric Micelles with Stimuli-Triggering Systems for Advanced Cancer Drug Targeting. *J. Drug Targeting.* **2014**, *22*, 584−599.
(18) Shi, Y.; van der Meel, R.; Theek, B.; Oude Blenke, E.; Pieters, E. H.; Fens, M. H.; Ehling, J.; Schiffelers, R. M.; Storm, G.; van Nostrum, C. F.; Lammers, T.; Hennink, W. E. Complete Regression of Xenograft Tumors upon Targeted Delivery of Paclitaxel via Pi-Pi Stacking Stabilized Polymeric Micelles. *ACS Nano* **2015**, *9*, 3740−3752.
(19) Harada, M.; Bobe, I.; Saito, H.; Shibata, N.; Tanaka, R.; Hayashi, T.; Kato, Y. Improved Anti-Tumor Activity of Stabilized Anthracycline Polymeric Micelle Formulation, NC-6300. *Cancer Sci.* **2011**, *102*, 192−199.
(20) Tsukioka, Y.; Matsumura, Y.; Hamaguchi, T.; Koike, H.; Moriyasu, F.; Kakizoe, T. Pharmaceutical and Biomedical Differences Between Micellar Doxorubicin (NK911) and Liposomal Doxorubicin (Doxil). *Jpn. J. Cancer Res.* **2002**, *93*, 1145−1153.
(21) Hofs, B.; Brzozowska, A.; de Keizer, A.; Norde, W.; Cohen Stuart, M. A. Reduction of Protein Adsorption to a Solid Surface by a Coating Composed of Polymeric Micelles with a Glass-Like Core. *J. Colloid Interface Sci.* **2008**, *325*, 309−315.
(22) Liu, S.; Wang, H.; Song, M.; Yin, J.; Jiang, G. Study of Protein Binding and Micellar Partition of Highly Hydrophobic Molecules in a Single System Using Capillary Electrophoresis. *Electrophoresis* **2008**, *29*, 3038−3046.
(23) Li, Y.; Budamagunta, M. S.; Luo, J.; Xiao, W.; Voss, J. C.; Lam, K. S. Probing of the Assembly Structure and Dynamics within Nanoparticles During Interaction with Blood Proteins. *ACS Nano* **2012**, *6*, 9485−9495.
(24) Saxer, T.; Zumbuehl, A.; Muller, B. The Use of Shear Stress for Targeted Drug Delivery. *Cardiovasc. Res.* **2013**, *99*, 328−333.
(25) Takahashi, A.; Ohkohchi, N.; Yasunaga, M.; Kuroda, J.; Koga, Y.; Kenmotsu, H.; Kinoshita, T.; Matsumura, Y. Detailed Distribution of NK012, an SN-38-Incorporating Micelle, in the Liver and its Potent Antitumor Effects in Mice Bearing Liver Metastases. *Clin. Cancer Res.* **2010**, *16*, 4822−4831.
(26) Chung, E. J.; Mlinar, L. B.; Sugimoto, M. J.; Nord, K.; Roman, B. B.; Tirrell, M. In Vivo Biodistribution and Clearance of Peptide Amphiphile Micelles. *Nanomedicine (N. Y., NY, U. S.)* **2015**, *11*, 479−487.
(27) Li, W.; Feng, S.; Guo, Y. Tailoring Polymeric Micelles to Optimize Delivery to Solid Tumors. *Nanomedicine (London, U. K.)* **2012**, *7*, 1235−1252.
(28) Xiao, K.; Luo, J.; Fowler, W. L.; Li, Y.; Lee, J. S.; Xing, L.; Cheng, R. H.; Wang, L.; Lam, K. S. A Self-Assembling Nanoparticle for Paclitaxel Delivery in Ovarian Cancer. *Biomaterials* **2009**, *30*, 6006−6016.
(29) Lu, J.; Huang, Y.; Zhao, W.; Marquez, R. T.; Meng, X.; Li, J.; Gao, X.; Venkataramanan, R.; Wang, Z.; Li, S. PEG−Derivatized Embelin as a Nanomicellar Carrier for Delivery of Paclitaxel to Breast and Prostate Cancers. *Biomaterials* **2013**, *34*, 1591−1600.
(30) Zhang, X.; Huang, Y.; Zhao, W.; Chen, Y.; Zhang, P.; Li, J.; Venkataramanan, R.; Li, S. PEG−Farnesyl Thiosalicylic Acid Telodendrimer Micelles as an Improved Formulation for Targeted Delivery of Paclitaxel. *Mol. Pharmaceutics* **2014**, *11*, 2807−2814.
(31) Zhang, X.; Lu, J.; Huang, Y.; Zhao, W.; Chen, Y.; Li, J.; Gao, X.; Venkataramanan, R.; Sun, M.; Stolz, D. B.; Zhang, L.; Li, S. PEG−Farnesylthiosalicylate Conjugate as a Nanomicellar Carrier for Delivery of Paclitaxel. *Bioconjugate Chem.* **2013**, *24*, 464−472.
(32) Cai, L.; Xu, G.; Shi, C.; Guo, D.; Wang, X.; Luo, J. Telodendrimer Nanocarrier for Co-Delivery of Paclitaxel and Cisplatin: A Synergistic Combination Nanotherapy for Ovarian Cancer Treatment. *Biomaterials* **2015**, *37*, 456−468.
(33) Xiao, W.; Luo, J.; Jain, T.; Riggs, J. W.; Tseng, H. P.; Henderson, P. T.; Cherry, S. R.; Rowland, D.; Lam, K. S. Biodistribution and Pharmacokinetics of a Telodendrimer Micellar Paclitaxel Nanoformulation in a Mouse Xenograft Model of Ovarian Cancer. *Int. J. Nanomed.* **2012**, *7*, 1587−1597.
(34) Lee, C. C.; MacKay, J. A.; Frechet, J. M.; Szoka, F. C. Designing Dendrimers for Biological Applications. *Nat. Biotechnol.* **2005**, *23*, 1517−1526.
(35) Wei, T.; Chen, C.; Liu, J.; Liu, C.; Posocco, P.; Liu, X.; Cheng, Q.; Huo, S.; Liang, Z.; Fermeglia, M.; Pricl, S.; Liang, X. J.; Rocchi, P.; Peng, L. Anticancer Drug Nanomicelles Formed by Self-Assembling Amphiphilic Dendrimer to Combat Cancer Drug Resistance. *Proc. Natl. Acad. Sci. U. S. A.* **2015**, *112*, 2978−2983.
(36) van Hest, J. C.; Delnoye, D. A.; Baars, M. W.; van Genderen, M. H.; Meijer, E. W. Polystyrene-Dendrimer Amphiphilic Block Copolymers with a Generation-Dependent Aggregation. *Science* **1995**, *268*, 1592−1595.
(37) van Tellingen, O.; Yetkin-Arik, B.; de Gooijer, M. C.; Wesseling, P.; Wurdinger, T.; de Vries, H. E. Overcoming the Blood-Brain Tumor Barrier for Effective Glioblastoma Treatment. *Drug Resist. Updates* **2015**, *19*, 1−12.
(38) Miura, Y.; Takenaka, T.; Toh, K.; Wu, S.; Nishihara, H.; Kano, M. R.; Ino, Y.; Nomoto, T.; Matsumoto, Y.; Koyama, H.; Cabral, H.; Nishiyama, N.; Kataoka, K. Cyclic RGD-Linked Polymeric Micelles for Targeted Delivery of Platinum Anticancer Drugs to Glioblastoma through the Blood-Brain Tumor Barrier. *ACS Nano* **2013**, *7*, 8583−8592.
(39) Cabral, H.; Matsumoto, Y.; Mizuno, K.; Chen, Q.; Murakami, M.; Kimura, M.; Terada, Y.; Kano, M. R.; Miyazono, K.; Uesaka, M.; Nishiyama, N.; Kataoka, K. Accumulation of Sub-100 nm Polymeric Micelles in Poorly Permeable Tumours Depends on Size. *Nat. Nanotechnol.* **2011**, *6*, 815−823.
(40) Li, J.; Zhou, L.; Ye, D.; Huang, S.; Shao, K.; Huang, R.; Han, L.; Liu, Y.; Liu, S.; Ye, L.; Lou, J.; Jiang, C. Choline-Derivate-Modified

DOI: 10.1021/acsami.5b07045
ACS Appl. Mater. Interfaces 2015, 7, 21589−21601

Nanoparticles for Brain-Targeting Gene Delivery. *Adv. Mater.* **2011**, *23*, 4516−4520.
(41) Li, J.; Guo, Y.; Kuang, Y.; An, S.; Ma, H.; Jiang, C. Choline Transporter-Targeting and Co-Delivery System for Glioma Therapy. *Biomaterials* **2013**, *34*, 9142−9148.
(42) Li, J.; Huang, S.; Shao, K.; Liu, Y.; An, S.; Kuang, Y.; Guo, Y.; Ma, H.; Wang, X.; Jiang, C. A Choline Derivate-Modified Nanoprobe for Glioma Diagnosis using MRI. *Sci. Rep.* **2013**, *3*, 1623.
(43) Gaillard, P. J.; Appeldoorn, C. C.; Dorland, R.; van Kregten, J.; Manca, F.; Vugts, D. J.; Windhorst, B.; van Dongen, G. A.; de Vries, H. E.; Maussang, D.; van Tellingen, O. Pharmacokinetics, Brain Delivery, and Efficacy in Brain Tumor-Bearing Mice of Glutathione Pegylated Liposomal Doxorubicin (2B3−101). *PLoS One* **2014**, *9*, e82331.
(44) Li, L.; Guan, Y.; Liu, H.; Hao, N.; Liu, T.; Meng, X.; Fu, C.; Li, Y.; Qu, Q.; Zhang, Y.; Ji, S.; Chen, L.; Chen, D.; Tang, F. Silica Nanorattle-Doxorubicin-Anchored Mesenchymal Stem Cells for Tumor-Tropic Therapy. *ACS Nano* **2011**, *5*, 7462−7470.
(45) Li, J.; Jiang, X.; Guo, Y.; An, S.; Kuang, Y.; Ma, H.; He, X.; Jiang, C. Linear-Dendritic Copolymer Composed of Polyethylene Glycol and All-Trans-Retinoic Acid as Drug Delivery Platform for Paclitaxel Against Breast Cancer. *Bioconjugate Chem.* **2015**, *26*, 418−426.
(46) Zhu, S.; Hong, M.; Tang, G.; Qian, L.; Lin, J.; Jiang, Y.; Pei, Y. Partly PEGylated Polyamidoamine Dendrimer for Tumor-Selective Targeting of Doxorubicin: the Effects of PEGylation Degree and Drug Conjugation Style. *Biomaterials* **2010**, *31*, 1360−1371.
(47) Ke, X.; Ng, V. W.; Ono, R. J.; Chan, J. M.; Krishnamurthy, S.; Wang, Y.; Hedrick, J. L.; Yang, Y. Y. Role of Non-Covalent and Covalent Interactions in Cargo Loading Capacity and Stability of Polymeric Micelles. *J. Controlled Release* **2014**, *193*, 9−26.
(48) Hodolic, M.; Michaud, L.; Huchet, V.; Balogova, S.; Nataf, V.; Kerrou, K.; Vereb, M.; Fettich, J.; Talbot, J. N. Consequence of the Introduction of Routine FCH PET/CT Imaging for Patients with Prostate Cancer: A Dual Centre Survey. *Radiol. Oncol.* **2014**, *48*, 20−28.
(49) Kwee, S. A.; DeGrado, T. R.; Talbot, J. N.; Gutman, F.; Coel, M. N. Cancer Imaging with Fluorine-18-Labeled Choline Derivatives. *Semin. Nucl. Med.* **2007**, *37*, 420−428.
(50) DeGrado, T. R.; Baldwin, S. W.; Wang, S.; Orr, M. D.; Liao, R. P.; Friedman, H. S.; Reiman, R.; Price, D. T.; Coleman, R. E. Synthesis and Evaluation of (18)F-Labeled Choline Analogs as Oncologic PET Tracers. *J. Nucl. Med.* **2001**, *42*, 1805−1814.
(51) Taguchi, C.; Inazu, M.; Saiki, I.; Yara, M.; Hara, N.; Yamanaka, T.; Uchino, H. Functional Analysis of [Methyl-(3)H]Choline Uptake in Glioblastoma Cells: Influence of Anti-Cancer and Central Nervous System Drugs. *Biochem. Pharmacol. (Amsterdam, Neth.)* **2014**, *88*, 303−312.
(52) Luwor, R. B.; Stylli, S. S.; Kaye, A. H. Using Bioluminescence Imaging in Glioma Research. *J. Clin. Neurosci.* **2015**, *22*, 779−784.
(53) Chlebowski, R. T. Adriamycin (Doxorubicin) Cardiotoxicity: A Review. *West. J. Med.* **1979**, *131*, 364−368.
(54) Zhang, Y. W.; Shi, J.; Li, Y. J.; Wei, L. Cardiomyocyte Death in Doxorubicin-Induced Cardiotoxicity. *Arch. Immunol. Ther. Exp.* **2009**, *57*, 435−445.

DOI: 10.1021/acsami.5b07045
ACS Appl. Mater. Interfaces 2015, 7, 21589−21601